IEEE Access
Multidisciplinary | Rapid Review | Open Access Journal

Received July 25, 2019, accepted August 5, 2019, date of publication August 22, 2019, date of current version September 3, 2019.

Digital Object Identifier 10.1109/ACCESS.2019.2936513

An Integrated Antenna System for 4G and Millimeter-Wave 5G Future Handheld Devices

SYEDA I. NAQVI[1], (Student Member, IEEE), AQEEL H. NAQVI[2], (Student Member, IEEE), FARZANA ARSHAD[1], MUHAMMAD A. RIAZ[1], (Member, IEEE), MUHAMMAD A. AZAM[3], (Member, IEEE), MANSOOR S. KHAN[4], YASAR AMIN[1], (Senior Member, IEEE), JONATHAN LOO[5], (Member, IEEE), AND HANNU TENHUNEN[6,7]

[1]ACTSENA Research Group, Telecommunication Engineering Department, University of Engineering and Technology, Taxila 47050, Pakistan
[2]School of Electrical and Electronics Engineering, Chung-Ang University, Seoul 06974, South Korea
[3]Department of Computer Engineering, University of Engineering and Technology, Taxila 47050, Pakistan
[4]Mathematics Department, COMSATS University Islamabad, Islamabad 45550, Pakistan
[5]School of Computing and Engineering, University of West London, London W5 5RF, U.K.
[6]Department of Electronic Systems, Royal Institute of Technology (KTH), SE 16440 Stockholm, Sweden
[7]Department of Information Technology, TUCS, University of Turku, 20520 Turku, Finland

Corresponding author: Syeda I. Naqvi (iffat.naqvi@uettaxila.edu.pk)

This work was supported in part by the Higher Education Commission (HEC) of Pakistan through Technology Development Fund under Grant TDF-67/2017, and in part by the ASR&TD-UETT faculty research grant.

ABSTRACT In this work, an integrated antenna system with Defected Ground Structure (DGS) is presented for Fourth Generation (4G) and millimeter (mm)-wave Fifth Generation (5G) wireless applications and handheld devices. The proposed design with overall dimensions of 110 mm × 75 mm is modeled on 0.508 mm thick Rogers RT/Duroid 5880 substrate. Radiating structure consists of antenna arrays excited by the T-shape 1 × 2 power divider/combiner. Dual bands for 4G centered at 3.8 GHz and 5.5 GHz are attained, whereas the 10-dB impedance bandwidth of 24.4 - 29.3 GHz is achieved for the 5G antenna array. In addition, a peak gain of 5.41 dBi is demonstrated across the operating bandwidth of the 4G antenna array. Similarly, for the 5G mm-wave configuration the attained peak gain is 10.29 dBi. Moreover, significant isolation is obtained between the two antenna modules ensuring efficient dual-frequency band operation using a single integrated solution. To endorse the concept, antenna prototype is fabricated and far-field measurements are procured. Simulated and measured results exhibit coherence. Also the proposed design is investigated for the beam steering capability of the mm-wave 5G antenna array using CST®MWS®. The demonstrated structure offers various advantages including compactness, wide bandwidth, high gain, and planar configuration. Hence, the attained radiation characteristics prove the suitability of the proposed design for the current and future wireless handheld devices.

INDEX TERMS Antenna array, integrated solution, 4G, mm-wave 5G, handheld devices.

I. INTRODUCTION

Rapidly increasing requirement in data rates prompted by modern wireless devices caused substantial development in establishing advanced standards for wireless communication systems [1]–[3]. In order to meet such high data requirements, modern wireless standards have adopted Long Term Evolution (LTE) and 4G standards for commercial and broadband wireless communication services [4]–[7]. Subsequently, researchers intensified their efforts on the next generation 5G wireless networks for mobile and broad-band wireless communication [8]–[12]. Henceforth the millimeter (mm)-wave radios have appeared as a significant solution for the 5G low-latency, multi-Gbps wireless networks [13]. The wireless devices supporting the future 5G communication applications must be proficient enough to operate at high data rates. This imminent standard for wireless communication requires wide bandwidth [14], [15]. Moreover, high gain is also essential to overcome the effects of raised atmospheric attenuations and absorptions at mm-wave frequencies [16], [17].

The associate editor coordinating the review of this article and approving it for publication was Adnan Shahid.

Antenna configuration consisting of a number of array elements providing high gain will be considered as an essential solution to this problem. Integrating the 4G at sub-6 GHz bands and 5G antennas at mm-wave frequencies will be an efficient solution for the future wireless communication applications. However, due to size restrictions, integrating such designs in handheld devices becomes difficult, as the coupling currents increase due to the nearby placement of adjacent antenna elements [18]. Thus sufficient isolation between antenna elements is necessary for such compact integrated designs.

5G wireless networks for broadband and cellular communication have drawn attention and intensive research has been carried out on designing antennas for mm-wave 5G communication applications. Recently reported work demonstrates numerous 5G antenna systems for mm-wave applications [19]–[21]. A four element mm-wave Multiple Input Multiple Output (MIMO) antenna with DGS is presented in [19], where the design acquires a gain value of 10.6 dB. Likewise, a 4 × 4 dual-band MIMO antenna with Electromagnetic Band Gap (EBG) structure is reported for 28 and 38 GHz future 5G wireless devices [20]. A smallest form factor Planar Inverted-F Antenna (PIFA) is reported in [21] for 5G applications. In this work, the obtained bandwidth for the dual bands is 3.34 GHz and 1.395 GHz respectively. Whereas, the gain attained is 3.75 dBi and 5.06 dBi, respectively.

Although there is continuous progress in mm-wave 5G antenna systems, it is required to employ the antenna array solutions in order to obtain a high gain. In addition, these high gain antenna systems should be pertinent and compatible with handheld terminals. Lately, a few antenna array solutions are reported with improved performance aiming 5G mm-wave applications [22]–[25]. In [22], a 4-element MIMO connected PIFA array for 28 GHz 5G mobile applications is presented, and the proposed structure is modeled with overall dimensions of 130 mm × 68 mm × 0.76 mm. Moreover, the peak gain obtained is 12 dBi. In the same way, a 16-element stacked array antenna with parasitic-patches is demonstrated for mm-wave 5G applications [23], where the geometrical size of the structure is 17.45 mm × 99.2 mm × 0.254 mm with maximum broadside gain of 19.88 dBi. Furthermore, an 8-element Vivaldi antenna array operating at 28 GHz is reported [24] with overall dimensions of 28.82 mm × 60 mm × 0.78 mm and the gain obtained is 11.2 dB. The work in [25], presents an 8-element antenna array for mobile application operating at 37-40 GHz with maximum gain of 12.2 dB, whereas the substrate size for the reported system is 130 mm × 65 mm × 0.25 mm.

The reported work discussed above is supporting either 4G LTE or 5G wireless communication applications. Subsequently, there is a need for a system that is compatible with both 4G and 5G technology. Recently, integrated antenna designs are reported supporting 4G and 5G wireless standards for mobile applications [26]–[30]. The work reported in [26] demonstrates an integrated 4G/5G antenna system acquiring peak gain of 4 and 8 dBi at microwave and mm-wave frequencies, respectively. Therefore, the design is suitable for smart phone devices with an overall size of 60 mm × 100 mm × 0.965 mm. Likewise, in [27] a connected MIMO antenna array system is presented for 4G/5G applications with 8 dBi peak gain value. In addition to this, a monopole based four-element MIMO antenna and a single connected antenna array with geometrical size of 115 mm × 65 mm × 0.76 mm is presented for the 4G and 28 GHz 5G applications [28]. Another MIMO 4G/5G antenna design is reported [29] for smart phones. The design is composed of 4-element monopoles for 4G and 2-element linear connected arrays for 5G with overall substrate size of 115 mm × 65 mm × 0.76 mm. In another work, a slot based connected antenna array with substrate size of 100 mm × 60 mm × 0.76 mm for typical modern mobile phone supporting 4G and 5G mm-wave wireless standards is demonstrated [30].

In this article, an integrated antenna design for the current 4G and the forthcoming 5G handheld devices is presented. The proposed structure is an arrangement of a two element antenna array for microwave frequency bands alongside a two element array for mm-wave frequency band. Also a sufficient bandwidth and gain is obtained for the acquired microwave and mm-wave frequency bands. Moreover, DGS is incorporated for the isolation enhancement amongst the antenna elements. Hence, the design with compact size while accomodating dual antenna systems is a potential candidate for future handheld applications.

II. DESIGN CONFIGURATION

Fig. 1 illustrates the layout of the integrated 4G/5G antenna system proposed in this work. The design consists of two antenna arrays, the one on the top side covers the microwave 4G bands whereas the other on the long edge of the board supports mm-wave 5G band as shown in Fig. 1 (a). CST®MWS® is used for the simulation and optimization purpose.

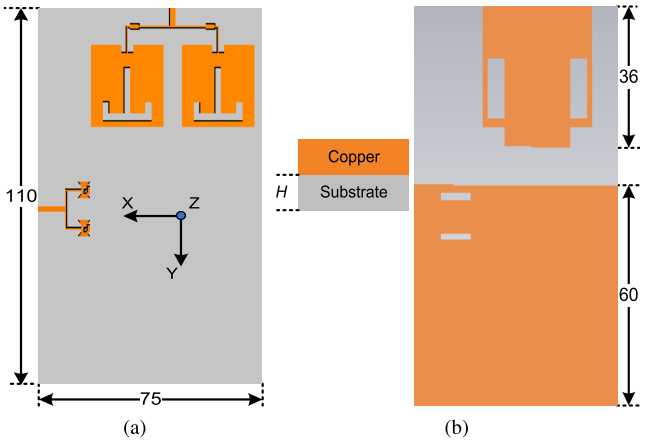

FIGURE 1. Layout of the proposed integrated antenna system (a) Front view, (b) Back view (All dimensions are in millimeter).

The design is realized on 0.508 mm thick Rogers RT/Duroid 5880 substrate with $\varepsilon_r = 2.2$, while the loss tangent,

δ is 0.0009. The overall dimensions of the substrate are 110 mm $\times$ 75 mm $\times$ 0.508 mm. The front side of the design in Fig. 1 (a) shows the feeding structure and port placement of the antenna arrays, whereas the back side shown in Fig. 1 (b) depicts the slotted ground plane.

The 4G antenna system consists of 1 $\times$ 2 antenna array excited by power divider/combiner. Optimization of the feeding structure and ground plane with DGS structure is carried out for improving the impedance matching. The 5G antenna array comprises of two elements. Also two horizontal slots are subtracted from the ground for enhanced impedance matching that leads to the good radiation characteristics. The optimized parameters for the proposed antenna system is tabulated in Table 1, and the design process is discussed below in detail.

TABLE 1. Optimized design parameters.

Name	Value(mm)	Name	Value(mm)
	4G Single Element Parameters		
L_p	22	L_{f1}	2.5
L_{f2}	6	L_{s1}	7
L_{s2}	2.5	W_p	17
W_{s1}	2	W_{s2}	2
W_{s3}	3		
	4G Array Parameters		
L	36	Lf	3
L_{f1}	6	L_{f2}	2
L_{g1}	30	L_{gs}	15
W_c	6	W	75
W_f	0.5	W_{gs}	6
W_{ge}	24	d	3
	5G Array Parameters		
L_{f1}	10	L_{f2}	4.5
L_{f3}	5	L_c	1
L_e	2	L_p	4.2
L_{g2}	60	L_s	1.7
W_{f1}	1.4	W_{f2}	0.5
W_p	3.5	W_{g2}	75
W_s	11	d_2	5.6

A. 4G ANTENNA DESIGN

The modeling of the design starts with a single element 4G antenna as shown in Fig. 2 (a). The inset-fed rectangular patch with inverted T-shaped slot is used as the elementary resonating component to acquire the benefits of low profile and planar structure. In the first place, single element antenna is designed by considering the following already established mathematical equations [31].

$$W_p = \frac{c}{2f_o}\sqrt{\frac{2}{(\varepsilon_r + 1)}} \tag{1}$$

$$L_p = \frac{c}{2f_o\sqrt{\varepsilon_{reff}}} - 2\Delta L \tag{2}$$

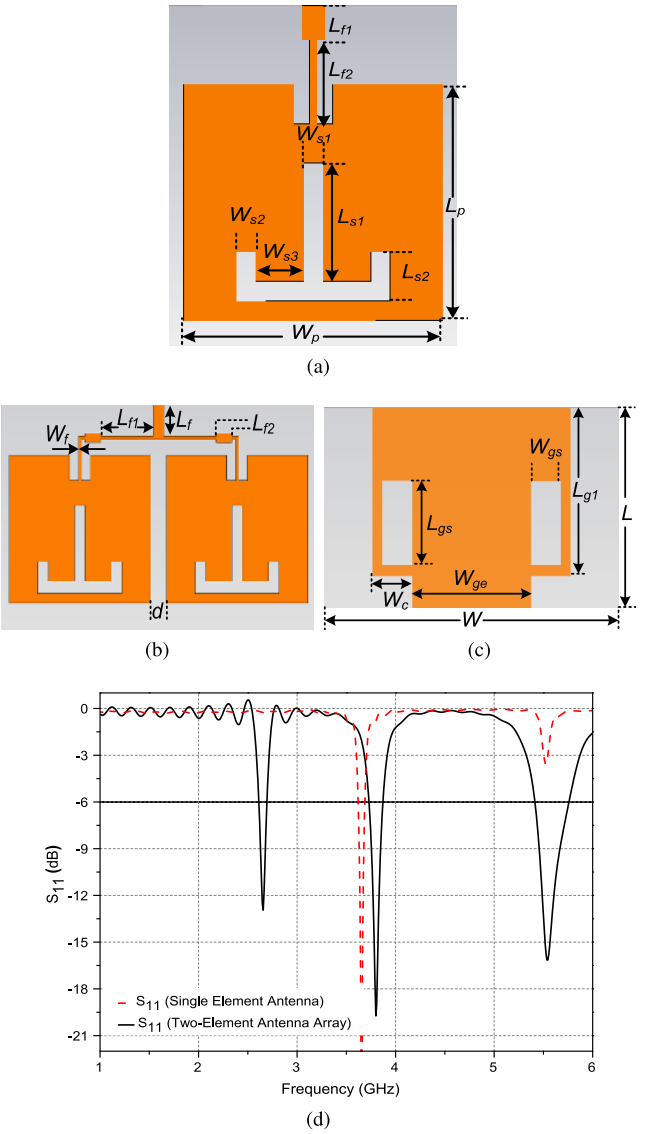

FIGURE 2. 4G Antenna design (a) Single element antenna, (b) Two-element antenna array, (c) Ground layer, (d) Simulated S_{11}.

where W_p and L_p is the width and length of the radiating patch, respectively, f_o is the operating frequency, ε_r is the relative dielectric constant and ΔL is the change in length due to fringing field effect which can be obtained using:

$$\Delta L = \frac{0.421H\left((\varepsilon_{reff} + 0.3)(\frac{W}{H} + 0.264)\right)}{\left((\varepsilon_{reff} - 0.258)(\frac{W}{H} + 0.8)\right)} \tag{3}$$

where ε_{reff} is given as:

$$\varepsilon_{reff} = \frac{\varepsilon_r + 1}{2} + \frac{\varepsilon_r - 1}{2}\frac{1}{\sqrt{(1 + 12\frac{H}{W})}} \tag{4}$$

where W and H is the width and height of the substrate respectively, whereas ε_{reff} is the effective permittivity.

Furthermore, the design is optimized from single element antenna to a two- element array with DGS as shown

in Fig. 2 (b) and (c). The design procedure of the 1 × 2 antenna array starts with a corporate feed combiner/splitter design. The two elements of the array are connected by a one-to-two parallel-feed network. Moreover, the quarter-wave matched T-junction power divider is employed to design the parallel-feed network for a balanced distribution of the input RF-power and impedance matching enhancement. In addition, the line widths of the feed network are calculated to match the main feed at impedance of 50Ω, while the branched network at 100Ω impedance. Hence, for impedance matching, the following microstrip transmission line characteristic equations are considered while modeling as follows [31].

For $\frac{W_f}{H} \leq 1$

$$Z_o = \frac{60}{\varepsilon_{reff}} \ln\left(\frac{8H}{W_f} + \frac{W_f}{4H}\right) \tag{5}$$

where

$$\varepsilon_{reff} = \frac{\varepsilon_r + 1}{2} + \frac{\varepsilon_r - 1}{2}\left(\frac{1}{\sqrt{1+12\frac{H}{W_f}}} + 0.04(1-\frac{W_f}{H})^2\right) \tag{6}$$

For $\frac{W_f}{H} \geq 1$

$$Z_o = \frac{120\pi\sqrt{\varepsilon_{reff}}}{\frac{W_f}{H} + 1.393 + 0.667\ln\left(\frac{W_f}{H} + 1.444\right)} \tag{7}$$

where

$$\varepsilon_{reff} = \frac{\varepsilon_r + 1}{2} + \frac{\varepsilon_r - 1}{2}\left(\frac{1}{\sqrt{1+12\frac{H}{W_f}}} + 0.04(1-12\frac{H}{W_f})^{\frac{-1}{2}}\right) \tag{8}$$

where Z_0 is the characteristic impedance of transmission line, and W_f is the width of the feed-line. The width and length of the feed network is calculated using the following equations:

$$W_f = \frac{2H}{\pi}\left(B-1+\frac{\varepsilon_r - 1}{2\varepsilon_r}\left[\ln(B-1)+0.39-\frac{0.61}{\varepsilon_r}\right]\right) \tag{9}$$

$$L_f = \frac{\lambda}{4\sqrt{\varepsilon_{reff}}} \tag{10}$$

$$B = \frac{60\pi^2}{Z_o\sqrt{\varepsilon_r}} \tag{11}$$

where B is a constant used in the inverse design formula, expressed in (9) for a microstrip line of a given characteristic impedance, and L_f is the length of the feedline. In order to achieve compactness, the distance d between the two elements is maintained at 3 mm which is approximately equal to 0.038λ for 3.8 GHz and 0.05λ for 5.5 GHz. In addition to this, alterations in the ground have been made by introducing two symmetrically placed vertical slots and truncated corners as illustrated in Fig. 2 (c), thus optimizing the reflection coefficient (S_{11}). The S_{11} curve for the single element 4G antenna in Fig. 2 (d) depicts that the achieved band is centered at 3.7 GHz with 90 MHz (−6 dB) bandwidth. For two- element array configuration, slight shifting of the band at 3.7 GHz to 3.8 GHz occurs, whereas two more bands are attained at 2.6 GHz and 5.5 GHz as shown in Fig. 2 (d). Consequently, the bandwidth of the band centered at 3.8 GHz increases from 90 MHz to 160 MHz.

B. MM-WAVE 5G ANTENNA DESIGN

At mm-wave frequencies, the antenna size is necessary to be compact. At first, the primary design of single element 5G antenna and feedline is obtained from (1-11). The optimized 5G antenna consists of rectangular shaped patch with trimmed corners and edges along with double bowtie slots at the centre of the patch as shown in Fig. 3 (a). Furthermore, the detailed dimensions of the 5G antenna are provided in Table 1. The simulated S_{22} curve for single element antenna shown in Fig. 3 (c) demonstrates that the covered band ranges from 27.3-28.6 GHz, with 1.3 GHz bandwidth. The miniaturization of the antenna and the increased amount

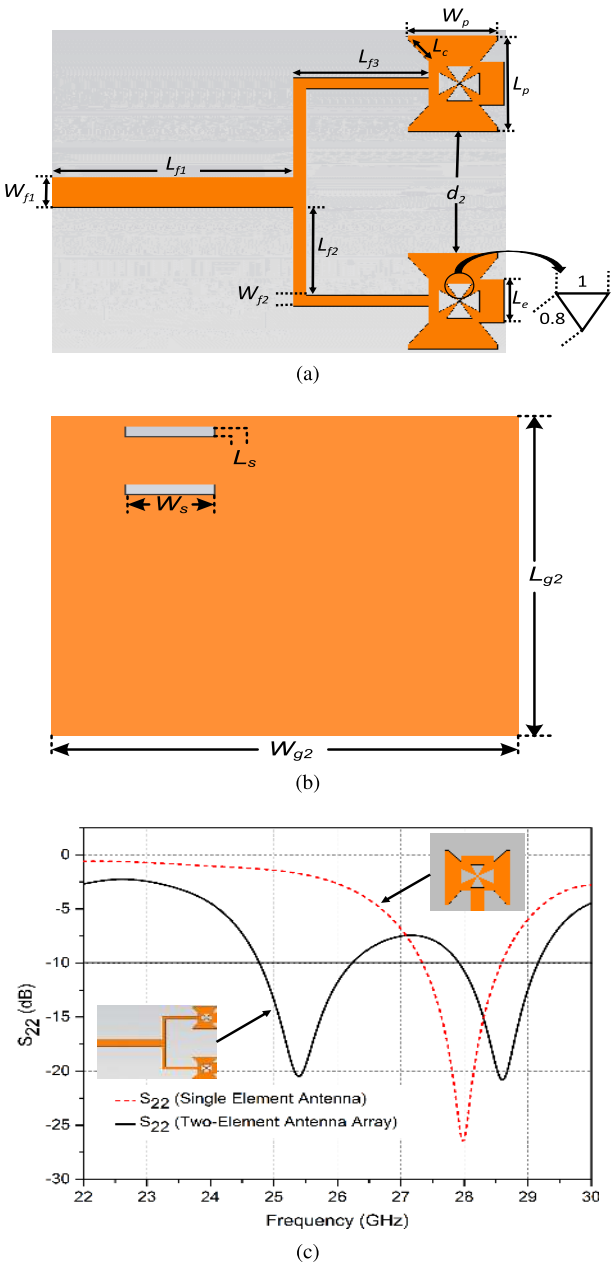

FIGURE 3. Two-element antenna array for 5G (a) Front view, (b) Back (Ground layer) view, (c) Simulated S_{22}.

of losses at higher frequencies require the use of antenna arrays to enhance the gain. Therefore in this work, a two-element antenna array is modeled as depicted in Fig. 3 (a), targeting the mm-wave 5G handheld terminals. The distance d_2 between the two array elements is 5.6 mm which is approximately equal to 0.47λ for 25.4 GHz and 0.54λ for 28.6 GHz frequencies. Aftewards, two horizontal slots are etched from the ground to improve the impedance matching as illustrated in Fig. 3 (b). The simulated S_{22} curve plotted in Fig. 3 (c) shows that the two-element antenna array covers 24.7-26.2 GHz and 27.9-29.2 GHz dual bands with 1.5 and 1.3 GHz (−10 dB) bandwidths, respectively.

C. 4G/5G INTEGRATED DESIGN

Afterwards, both the 4G and 5G antenna arrays are integrated on the same board and subsequent effects are investigated. The layout of the integrated 4G/5G antenna design is depicted in Fig. 4. The antenna arrays supporting 4G and 5G frequency bands are placed on the top side and along the long edge of the board, respectively, as illustrated in Fig. 4 (a). Likewise, the ground layer of the integrated design is shown in Fig. 4 (b). Therefore, the compact structure as well as the placement of the antenna modules demonstrates the suitability of the proposed design for current and future handheld devices [32].

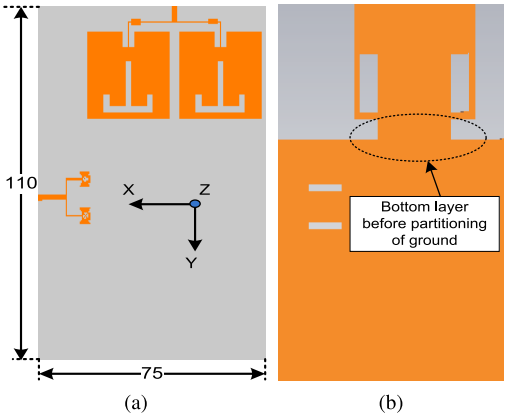

FIGURE 4. Layout of the integrated antenna system before optimization (a) Front view, (b) Back view.

The S_{11} curve for 4G microwave frequencies in Fig. 5 (a) demonstrates that as a result of integrating both antenna modules, band at 3.8 GHz shifts upward (with $S_{11} > -10$ dB). Moreover, the bandwidth of the 5.5 GHz band narrows down from 350 to 300 MHz. Similarly, at 5G mm-wave frequencies, the integration results in attainment of a wideband covering 25.3-28.6 GHz frequency band as shown in Fig. 5 (b). Hence, the bandwidth achieved for this wideband is 3.3 GHz.

To further improve the results, it was required to optimize the design. After carrying out parametric analysis, the design is modified by segregating the ground into two parts. The final optimized design of the overall integrated antenna system is shown earlier in Fig. 1 (a) and (b). Likewise, the S-parameter curves for the optimized integrated 4G/5G antenna design are

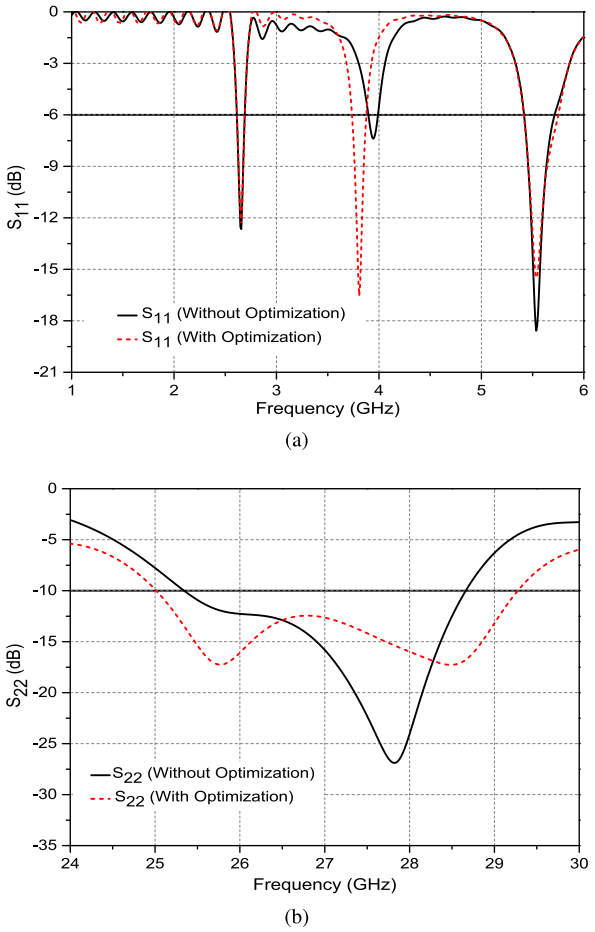

FIGURE 5. Simulated S-parameter curves of integrated design with and without optimization (a) S_{11} for two-element 4G antenna array, (b) S_{22} for two- element 5G antenna array.

illustrated in Fig. 5 (a) and (b) for the sub-6 GHz as well as mm-wave frequency band, respectively. The optimized results show that band at 3.8 GHz shifts downward with $S_{11} < -10$ dB as well as an improved bandwidth of 170 MHz is obtained. In addition, the bandwidth for the 5.5 GHz band improves from 300 to 360 MHz. In the same manner, the S-parameter curve for the mm-wave frequencies in Fig. 5 (b) illustrates that after design modification a wide band covering 25-29.3 GHz has been obtained with 4.3 GHz (−10 dB) bandwidth.

The simulated isolation curves in Fig. 6 (a) and (b) demonstrates that isolation has been enhanced after the modification of ground. Henceforth, an improvement in minimum isolation is observed from 40 dB to 43 dB for the obtained microwave frequency bands, whereas for the mm-wave frequency band, minimum isolation is improved from 38 dB to about 43 dB between the two ports.

The radiating behavior of the antenna array elements is further investigated by observing the surface current distribution. The objective for carrying out this analysis is to ascertain the antenna parts that are radiating and to elucidate the coupling amongst adjacent elements. Initially, the port 1 is

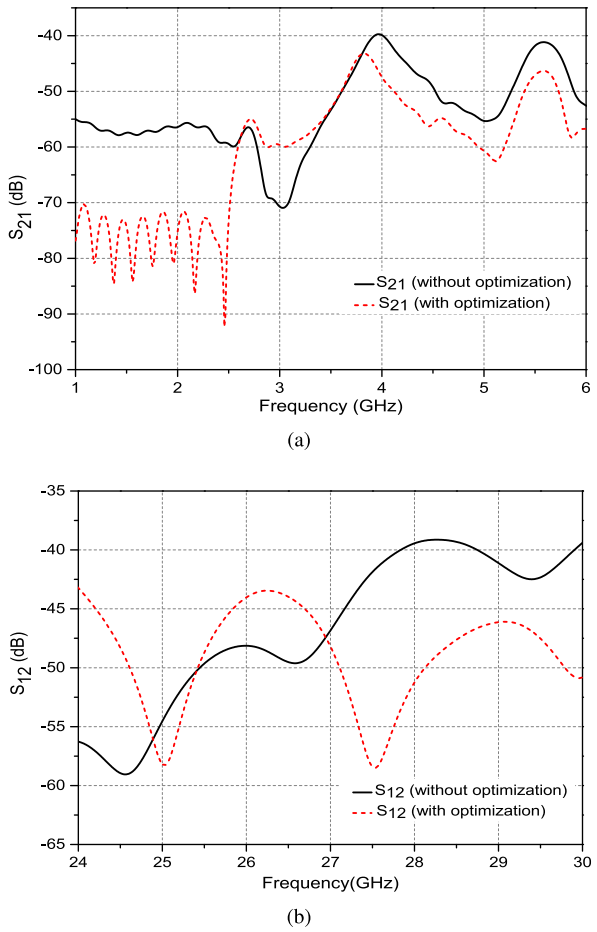

FIGURE 6. Simulated isolation curves of integrated design with and without optimization (a) S_{21} for two-element 4G antenna array, (b) S_{12} for two-element 5G antenna array.

activated at 3.8 GHz and 5.5 GHz as shown in Fig. 7. For 3.8 GHz, a high surface current is observed along the inverted T-slot, as illustrated in Fig. 7 (a). Whereas, for 5.5 GHz resonant frequency, the maximum current distribution is noticed around the vertical slots in the ground plane, as demonstrated in Fig. 7 (b). This illustrates the impact of ground in radiation behavior. Moreover, insignificant coupling amid the two adjacent 4G antenna array elements is also observed. In order to understand the radiation mechanism of the antenna array at mm-wave frequencies, current distribution at 28 GHz is examined by activating the port 2, as shown in Fig.7 (c). It is observed that at 28 GHz, surface current is strongly concentrated on the feedline as well as around the bowtie slots in the patch. Likewise, concentration of current around the horizontal slots in the ground demonstrates the significant amount of coupling between the slots and the feed line, which mainly contributes to the added resonances ultimately forming a wideband.

III. RESULTS AND DISCUSSION

The proposed integrated antenna array solution is fabricated on a Rogers RT/Duroid 5880 Substrate using the photolithography process to experimentally exhibit the concept.

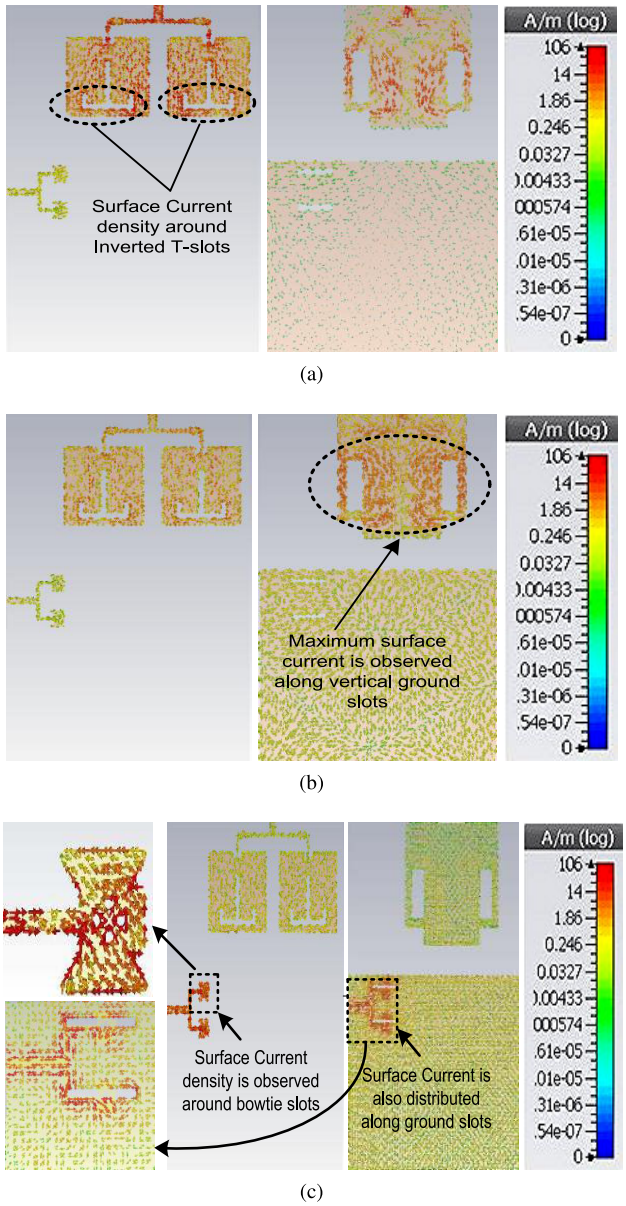

FIGURE 7. Current distribution at (a) 3.8 GHz, (b) 5.5 GHz, and (c) 28 GHz.

A 50Ω subMiniature version A (SMA) connector is connected to each antenna array as shown in Fig. 8 (a). Fig. 8. (a) and (b) illustrates the fabricated prototype and the farfield measurement setup respectively. The measured results are discussed below.

A. SCATTERING PARAMETERS

The S-parameters of the fabricated prototype were measured using the Rohde & Schwarz ZVA 40 Vector Network Analyzer. Fig. 9. (a) - (d), shows the measured and simulated S-parameter curves for the proposed integrated 4G and 5G antenna system. The S_{11} curve demonstrates that the 4G antenna system is resonating at 3.8 and 5.5 GHz with sufficient bandwidths of 160 MHz and 450 MHz respectively,

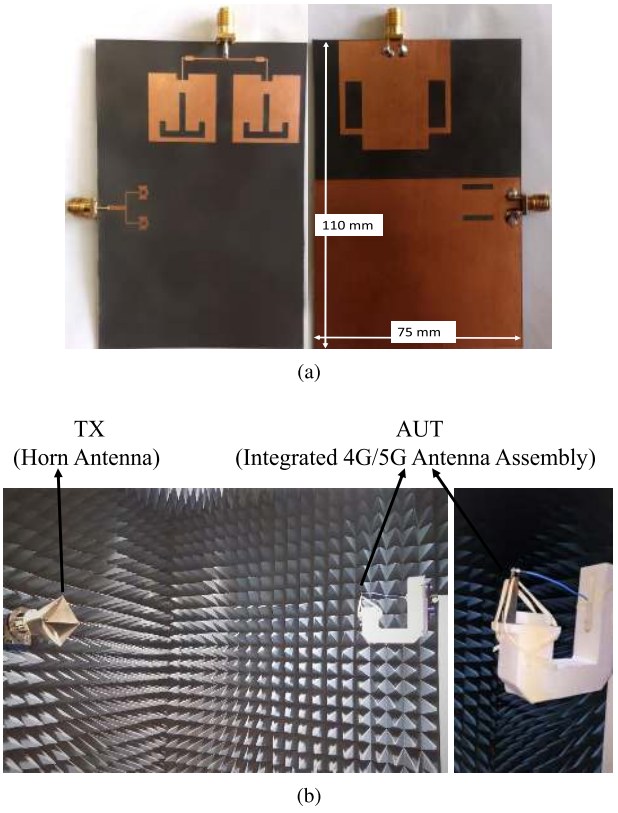

FIGURE 8. (a) Fabricated prototype, (b) Far-field measurement setup.

as illustrated in Fig. 9 (a). As a result of comparing simulated and measured results, an increase in bandwidth for the 5.5 GHz operating band is observed. On the otherhand, the band at 2.6 GHz shifts upward (with S_{11}>−6 dB), therefore this band is not claimed as an operational band. Additionally, the minimum measured isolation at the sub-6 GHz band is 41 dB between two ports, whereas the simulated isolation is approximately 43 dB as shown in Fig. 9 (b).

The simulated as well as measured S-parameter curves of the proposed mm-wave 5G antenna system are shown in Fig. 9 (c) and (d). The measured and simulated 10-dB impedance bandwidths are 24.4-29.3 GHz and 25-29.3 GHz, respectively. Therefore, the measured bandwidth of 4.9 GHz is obtained for the mm-wave frequency band. Furthermore, the measured isolation at mm-wave frequency band is approximately 38 dB as compared to the simulated isolation that is nearly 43 dB. Therefore, the measured and simulated results are in good coherence. While, the insignificant difference is due to the fabrication errors and inevitable use of coaxial cables for measurement purpose [33], [34].

B. RADIATION PATTERNS

The 3D radiation patterns of the antenna for microwave frequencies at sub-6 GHz band, are measured using the commercial ORBIT/FR far-field measurement system in a shielded radio frequency anechoic chamber as shown in Fig. 8 (b).

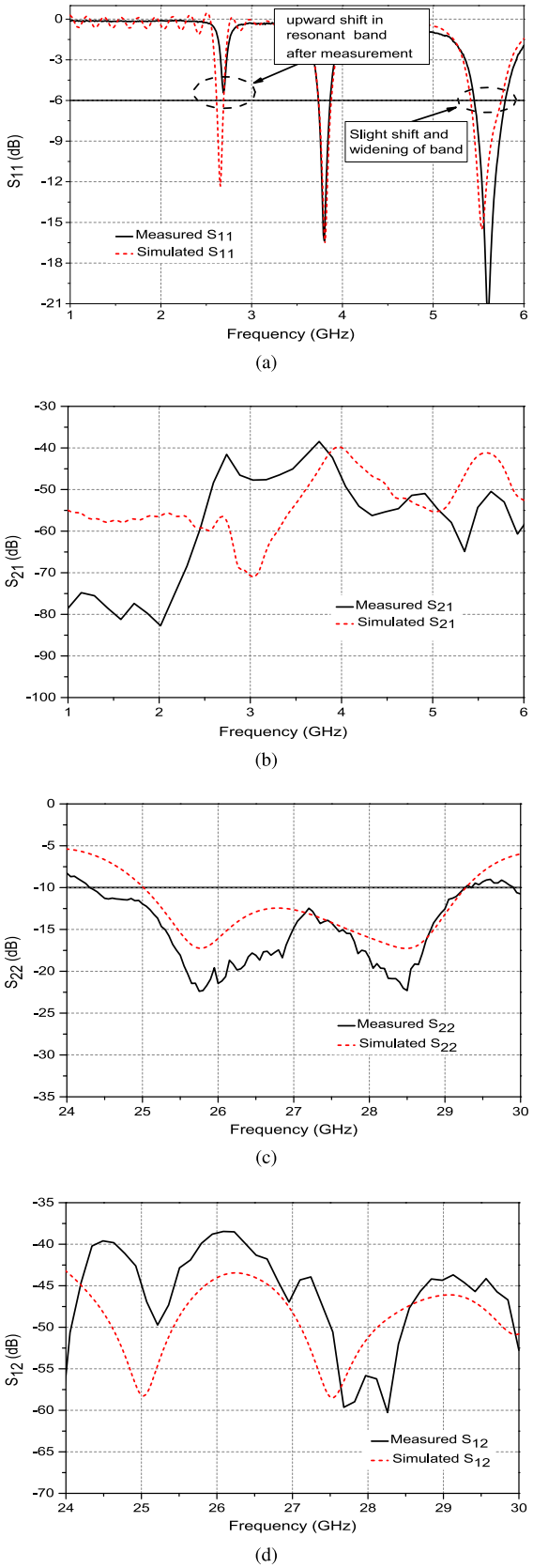

FIGURE 9. Measured and simulated S-parameter curves of integrated design (a) S_{11} for two-element 4G array, (b) S_{21} for two-element 4G array, (c) S_{22} for two-element 5G array, (d) S_{12} for two-element 5G array.

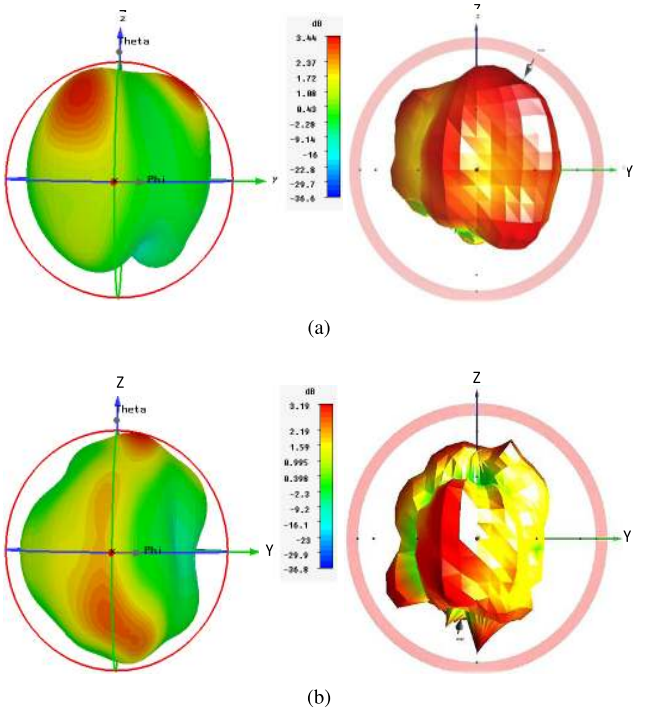

FIGURE 10. Simulated (left) and measured (right) 3D radiation patterns at (a) 3.8 GHz, (b) 5.5 GHz.

As a result, the 3-D radiation patterns are obtained at 3.8 and 5.5 GHz as shown in Fig. 10 (a) and (b) respectively. The Antenna Under Test (AUT) is rotated to obtain the radiation intensity of the antenna at different orientations. It can be seen that the antenna exhibit nearly a directional radiation pattern.

For mm-wave frequency, the far-field radiation patterns are measured for the theta values ranging from $-90°$ to $90°$. The transmit horn antenna used is SGH-series (SGH-15) by Millitech Co. which has a standard gain of 24 dBi. The simulated and measured 2D radiation patterns at 28.25 GHz in xz and yz plane are depicted in Fig. 11 (a) and (b), respectively. The maximum radiation is observed at $\theta = -15°$ for xz plane, whereas an observation at $\theta = 9°$ is made for the yz plane.

C. GAIN AND EFFICIENCIES

The gain and efficiencies of the integrated antenna system at different frequencies are tabulated in Table 2. The measured peak gain of 3.27 dBi and 5.41 dBi is achieved at 3.8 and 5.5 GHz frequencies, respectively. Likewise, a maximum gain of 10.29 dBi is obtained at 28.25 GHz. Additionally, a maximum efficiency of 79% is obtained for the 4G antenna array whereas, for 5G antenna array maximum obtained efficiency is 71%. However, some inconsistencies have been observed between the simulated and the measured results which are primarily due to the imperfections in the fabrication of the antenna and the connectors used.

The proposed antenna solution is compared in Table 3 with the related work [26], [27], and [29] reported in literature. Thus, it can be seen that the design complexity is low for the proposed antenna. Moreover, the significance of the proposed antenna system as compared to the other designs is evident in terms of achieved high gain over a wider bandwidth. Therefore, this proves the suitability of antenna design for future handheld devices.

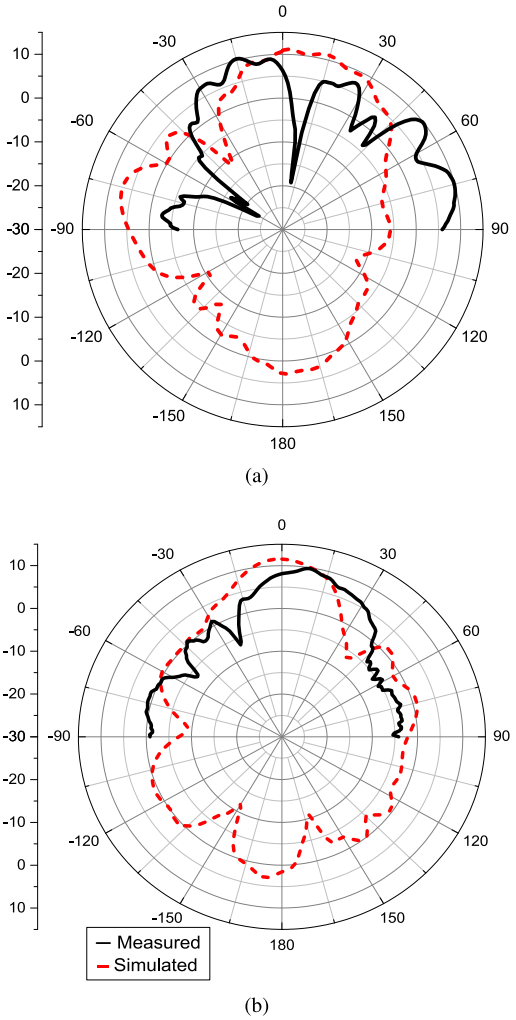

FIGURE 11. Measured and simulated 2D radiation patterns at 28.25 GHz (a) XZ plane, (b) YZ plane.

TABLE 2. Gain and efficiencies of 4G/5G antenna system.

Frequency(GHz)	Peak Gain(dB)		Efficiency(%)	
	Simulated	Measured	Simulated	Measured
3.8	3.44	3.27	79	71
5.5	3.19	5.41	75	79
28	9.90	8.77	68	65
28.25	10.10	10.29	69	71
28.5	10.31	9.51	75	63
28.75	10.50	9.86	77	69
29	10.72	9.95	79	70

IV. BEAM STEERING PERFORMANCE ANALYSIS

Research in beam steerable antennas is gaining a lot of attention as efforts are being made to obtain an optimal

TABLE 3. Comparison with the literature designs.

Ref.	Substrate Size	Freq. bands (GHz)	Bandwidth (GHz)	Peak Gain (dBi)	Efficiency(%)
Rifaqat et.al.[26]	100 mm×60 mm×0.965 mm	1.8-2.5, 26.7-28.4	0.7, 1.7	3.8, 8	
Sharawi et.al.[27]	100 mm×60 mm×0.76 mm	1.9-2.0, 2.16-2.23, 2.35-2.62, 3.06-3.14, 16.50-17.80	0.1, 0.07, 0.27, 0.08, 1.3	2.22, 8	
Muhammad et.al.[29]	115 mm×65 mm×0.76 mm	1.9-3.2, 3.5-3.7, 25.7–30.5	1.3, 0.2, 4.8	5.1, 9.9	
Proposed Design	110 mm×75 mm×0.508 mm	3.73-3.89, 5.40-5.85	0.16,0.45	3.27 , 5.41	71, 79
		24.4-29.3	4.9	10.29	71

beam steering solution at mm-wave frequency band for both point-to-point and point-to-multipoint applications. Higher propagation losses at mm-wave frequencies that prominently vary depending on the environment require antenna arrays with beam steering capability, as it increases the capacity of cellular networks by improving the signal to interference ratio (SIR) through direct targeting of user groups. Thus beam steerable antennas are critical for increasing spectral efficiencies and will play an important role in 5G implementations [10].

Beam steering permits an antenna system containing a number of individual antennas to have the direction of the beam to be changed by altering the phase and amplitude of the signals provided to the individual antenna elements. With increasing number of radiating elements in the array, the beam becomes narrower and more directional. A linear phased array with equal spaced elements is easiest to analyze and forms the basis for most array designs with beam steering ability.

A beam steerable antenna array can be created by using a number of closely spaced antenna elements. If the antenna elements are equally spaced, then phase shift between the antenna elements is calculated using equation provided below [35].

$$\Psi = \frac{2\Pi d_e(sin\theta)}{\lambda} \tag{12}$$

where Ψ is the phase difference between two adjacent beams, d_e is the array element spacing, λ is the wavelength, and θ is the pointing angle. A variety of techniques have been used to steer an antenna's radiation, including mechanical steering, parasitic steering, Integrated Lens Antennas (ILAs), switched beam antennas using PIN-diode and varactor diode [36]–[40].

For the proof of concept, the beam steering capability of the proposed mm-wave antenna array is investigated by manually introducing the phase shift to each element of the antenna array using CST®MWS®. At first place, an array of two radiating elements is excited by a signal of distinct phase and amplitude. The simulated radiation patterns at 28.25 GHz with different phase shifting values demonstrates the main beam direction at $-16°$, $0°$, and $+19°$. Afterwards, an array configuration with four elements separated by distance d_e (0.5λ) as shown in Fig. 12, is investigated and scan angles of $-17°$, $0°$, and $+19°$ are observed. It is also evident from

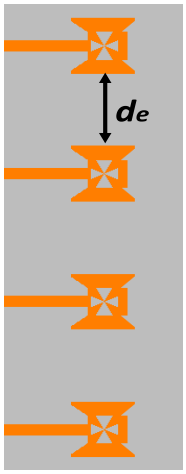

FIGURE 12. Design of four element antenna array for mm-wave frequencies.

Fig. 13 (a) and (b) that the peak gain of the array has increased with increasing number of elements. Thus a narrower and more directional beam is obtained for four-element array as compared to two-element array. For eight element antenna array, the radiation pattern in Fig. 13 (c) illustrates scan angles of $-28°$, $0°$, and $+29°$ for different phase values. It is also observed that the radiation pattern for the eight element array is not steering significantly. Since the beam width of the antenna radiation pattern is dependent on the phase constant "β", and β varies relatively with attenuation constant "α", therefore when the attenuation constant becomes equal or closer to phase constant, the beam get split and becomes wider [41]. Thus in order to avoid the beam splitting and to obtain a steerable beam, the aperture size or attenuation constant could be adjusted. The scan angles and peak gain values for different array configurations are also provided in Table 4.

TABLE 4. Beam steerable array performance metrics.

No. of Elements	Scan Angle (degree)	Peak Gain(dBi)
2 elements	-16°, 0°, +19°	11.3
4 elements	-17°, 0°, +19°	14.7
8 elements	-28°, 0°, +29°	15.4

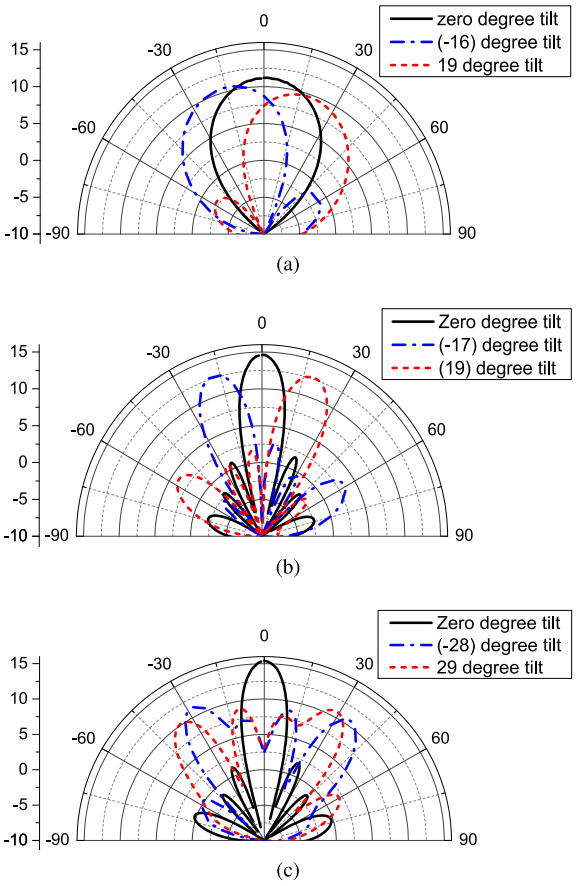

FIGURE 13. Simulated radiation patterns at 28.25 GHz for (a) Two element antenna array, (b) Four element antenna array, (c) Eight element antenna array.

Although the beam steering capability is demonstrated at a very basic level and just for the proof of concept in this work, more sophisticated techniques to introduce phase shifts will be explored in the future.

V. CONCLUSION

This work demonstrates an integrated antenna design supporting current 4G and future 5G wireless communication systems. The integrated solution consists of two antenna arrays excited by the T-junction power divider/combiner. The 4G antenna array covers the dual sub-6 GHz frequency bands centered at 3.8 GHz and 5.5 GHz with measured bandwidths of 160 and 450 MHz respectively. Whereas, the 5G antenna array supports mm-wave 26/28 GHz frequency bands with wide bandwidth of 4.9 GHz. In addition, the peak gain values of 3.27 and 5.41 dBi are attained for 4G antenna. Likewise, for mm-wave 5G antenna, a maximum gain value of 10.29 dBi is achieved. Beam steering capability of the proposed 5G mm-wave antenna is also investigated using CST®MWS® by manullay altering the phase of the antenna elements for two, four and eight element array configurations. The radiated beam is steered in an elevated plane at $-17°$, $0°$ and $+19°$. Moreover, an enhanced isolation is obtained due to DGS. Measured and simulated results exhibit good agreement. Therefore, the proposed single layered, compact and low profile antenna solution is a suitable contender for the present 4G and forthcoming 5G enabled wireless handheld devices.

ACKNOWLEDGMENT

The authors would like to thank National Institute of Electronics (NIE), Islamabad, Pakistan for the design fabrication services. The authors would also like to thank Electromagnetic Waves Technology Institute (EMTI), Yongsan-gu, Seoul, South Korea for testing services.

REFERENCES

[1] I. F. Akyildiz, D. M. Gutierrez-Estevez, and E. C. Reyes, "The evolution to 4G cellular systems: LTE-advanced," *Phys. Commun.*, vol. 3, no. 4, pp. 217–244, 2010.
[2] M. Rinne and O. Tirkkonen, "LTE, the radio technology path towards 4G," *Comput. Commun.*, vol. 33, no. 16, pp. 1894–1906, 2010.
[3] C. Zhang, S. L. Ariyavisitakul, and M. Tao, "LTE-advanced and 4G wireless communications [guest editorial]," *IEEE Commun. Mag.*, vol. 50, no. 2, pp. 102–103, Feb. 2012.
[4] Y.-L. Ban, J.-H. Chen, S. Yang, J. L.-W. Li, and Y.-J. Wu, "Low-profile printed octa-band LTE/WWAN mobile phone antenna using embedded parallel resonant structure," *IEEE Trans. Antennas Propag.*, vol. 61, no. 7, pp. 3889–3894, Jul. 2013.
[5] J.-H. Lu and J.-L. Guo, "Small-size octaband monopole antenna in an LTE/WWAN mobile phone," *IEEE Antennas Wireless Propag. Lett.*, vol. 13, pp. 548–551, 2014.
[6] H. Chen and A. Zhao, "LTE antenna design for mobile phone with metal frame," *IEEE Antennas Wireless Propag. Lett.*, vol. 15, pp. 1462–1465, 2016.
[7] Y. Wang and Z. Du, "Wideband monopole antenna with less nonground portion for octa-band WWAN/LTE mobile phones," *IEEE Trans. Antennas Propag.*, vol. 64, no. 1, pp. 383–388, Jan. 2016.
[8] J. G. Andrews, S. Buzzi, W. Choi, S. V. Hanly, A. Lozano, A. C. K. Soong, and J. C. Zhang, "What will 5G be?" *IEEE J. Sel. Areas Commun.*, vol. 32, no. 6, pp. 1065–1082, Jun. 2014.
[9] M.-Y. Li, Y.-L. Ban, Z.-Q. Xu, G. Wu, C.-Y.-D. Sim, and K. Kang, "Eight-port orthogonally dual-polarized antenna array for 5G smartphone applications," *IEEE Trans. Antennas Propag.*, vol. 64, no. 9, pp. 3820–3830, Sep. 2016.
[10] A. H. Naqvi and S. Lim, "Review of recent phased arrays for millimeter-wave wireless communication," *Sensors*, vol. 18, no. 10, p. 3194, 2018.
[11] Y. Li, C.-Y.-D. Sim, Y. Luo, and G. Yang, "Multiband 10-antenna array for sub-6 GHz MIMO applications in 5-G smartphones," *IEEE Access*, vol. 6, pp. 28041–28053, 2018.
[12] K.-L. Wong, C.-Y. Tsai, and J.-Y. Lu, "Two asymmetrically mirrored gap-coupled loop antennas as a compact building block for eight-antenna MIMO array in the future smartphone," *IEEE Trans. Antennas Propag.*, vol. 65, no. 4, pp. 1765–1778, Apr. 2017.
[13] T. S. Rappaport, S. Sun, R. Mayzus, H. Zhao, Y. Azar, K. Wang, G. N. Wong, J. K. Schulz, M. Samimi, and F. Gutierrez, "Millimeter wave mobile communications for 5G cellular: It will work!" *IEEE Access*, vol. 1, pp. 335–349, May 2013.
[14] W. Hong, K.-H. Baek, Y. Lee, Y. Kim, and S.-T. Ko, "Study and prototyping of practically large-scale mmWave antenna systems for 5G cellular devices," *IEEE Commun. Mag.*, vol. 52, no. 9, pp. 63–69, Sep. 2014.
[15] W. Hong, K.-H. Baek, and S. Ko, "Millimeter-wave 5G antennas for smartphones: Overview and experimental demonstration," *IEEE Trans. Antennas Propag.*, vol. 65, no. 12, pp. 6250–6261, Dec. 2017.
[16] J. Zhang, X. Ge, Q. Li, M. Guizani, and Y. Zhang, "5G millimeter-wave antenna array: Design and challenges," *IEEE Wireless Commun.*, vol. 24, no. 2, pp. 106–112, Apr. 2017.
[17] I. Shayea, T. A. Rahman, M. H. Azmi, and M. R. Islam, "Real measurement study for rain rate and rain attenuation conducted over 26 GHz microwave 5G link system in Malaysia," *IEEE Access*, vol. 6, pp. 19044–19064, 2018.

[18] Y. Kim and W. Hong, "Coexistance issues concerning 4G and mmwave 5G antennas for mobile terminals," in *Proc. 6th Asia–Pacific Conf. Antennas Propag. (APCAP)*, Oct. 2017, pp. 1–3.
[19] S. F. Jilani and A. Alomainy, "Millimetre-wave T-shaped MIMO antenna with defected ground structures for 5G cellular networks," *IET Microw., Antennas Propag.*, vol. 12, no. 5, pp. 672–677, Apr. 2018.
[20] D. T. T. Tu, N. G. Thang, N. T. Ngoc, N. T. B. Phuong, and V. Van Yem, "28/38 GHz dual-band MIMO antenna with low mutual coupling using novel round patch EBG cell for 5G applications," in *Proc. IEEE Int. Conf. Adv. Technol. Commun. (ATC)*, Oct. 2017, pp. 64–69.
[21] W. Ahmad and W. T. Khan, "Small form factor dual band (28/38 GHz) PIFA antenna for 5G applications," in *IEEE MTT-S Int. Microw. Symp. Dig.*, Mar. 2017, pp. 21–24.
[22] M. Ikram, Y. Wang, M. S. Sharawi, and A. Abbosh, "A novel connected PIFA array with MIMO configuration for 5G mobile applications," in *Proc. Austral. Microw. Symp. (AMS)*, Feb. 2018, pp. 19–20.
[23] M. Khalily, R. Tafazolli, P. Xiao, and A. A. Kishk, "Broadband mm-wave Microstrip array antenna with improved radiation characteristics for different 5G applications," *IEEE Trans. Antennas Propag.*, vol. 66, no. 9, pp. 4641–4647, Sep. 2018.
[24] S. Zhu, H. Liu, Z. Chen, and P. Wen, "A compact gain-enhanced Vivaldi antenna array with suppressed mutual coupling for 5G mmWave application," *IEEE Antennas Wireless Propag. Lett.*, vol. 17, no. 5, pp. 776–779, May 2018.
[25] M. Peng and A. Zhao, "High performance 5G millimeter-wave antenna array for 37–40 GHz mobile application," in *Proc. Int. Workshop Antenna Technol. (iWAT)*, Mar. 2018, pp. 1–4.
[26] R. Hussain, A. T. Alreshaid, S. K. Podilchak, and M. S. Sharawi, "Compact 4G MIMO antenna integrated with a 5G array for current and future mobile handsets," *IET Microw., Antennas Propag.*, vol. 11, no. 2, pp. 271–279, 2017.
[27] M. S. Sharawi, M. Ikram, and A. Shamim, "A two concentric slot loop based connected array MIMO antenna system for 4G/5G terminals," *IEEE Trans. Antennas Propag.*, vol. 65, no. 12, pp. 6679–6686, Dec. 2017.
[28] M. Ikram, M. S. Sharawi, and A. Shamim, "A novel very wideband integrated antenna system for 4G and 5G mm-wave applications," *Microw. Opt. Technol. Lett.*, vol. 59, no. 12, pp. 3082–3088, 2017.
[29] M. Ikram, M. S. Sharawi, A. Shamim, and A. Sebak, "A multiband dual-standard MIMO antenna system based on monopoles (4G) and connected slots (5G) for future smart phones," *Microw. Opt. Technol. Lett.*, vol. 60, no. 6, pp. 1468–1476, 2018.
[30] M. S. Sharawi and M. Ikram, "Slot-based connected antenna arrays for 5G mobile terminals," in *Proc. Int. Workshop Antenna Technol. (iWAT)*, Mar. 2018, pp. 1–3.
[31] C. A. Balanis, *Antenna Theory: Analysis and Design*, 3rd ed. Hoboken, NJ, USA: Wiley, 2005.
[32] Apple. *Accessory Design Guidelines for Apple Devices*. Accessed: Mar. 29, 2019. [Online]. Available: https://developer.apple.com/accessories/Accessory-Design-Guidelines.pdf
[33] L. Liu, S. W. Cheung, Y. F. Weng, and T. I. Yuk, "Cable effects on measuring small planar UWB monopole antennas," in *Ultra Wideband Current Status and Future Trends*. London, U.K.: InTech, 2012, ch. 12. doi: 10.5772/46080.
[34] L. Liu, Y. F. Weng, S. W. Cheung, T. I. Yuk, and L. J. Foged, "Modeling of cable for measurements of small monopole antennas," in *Proc. Loughborough Antennas Propag. Conf. (LAPC)*, Loughborough, U.K., Nov. 2011, pp. 1–4.
[35] R. J. Mailloux, *Phased Array Antenna Handbook*, 2nd ed. Norwood, MA, USA: Artech House, 2005.
[36] A. V. Räisänen, J. Ala-Laurinaho, D. Chicherin, Z. Du, A. Generalov, A. Karttunen, D. Lioubtchenko, J. Mallat, A. Tamminen, and T. Zvolensky, "Beam-steering antennas at millimeter wavelengths," in *Proc. 5th Global Symp. Millim.-Waves*, May 2012, pp. 170–173.
[37] A. Artemenko, A. Mozharovskiy, A. Maltsev, R. Maslennikov, A. Sevastyanov, and V. Ssorin, "2D electronically beam steerable integrated lens antennas for mmWave applications," in *Proc. 42nd Eur. Microw. Conf.*, Oct./Nov. 2012, pp. 213–216.
[38] M. Bouslama, M. Traii, T. A. Denidni, and A. Gharsallah, "Beam-switching antenna with a new reconfigurable frequency selective surface," *IEEE Antennas Wireless Propag. Lett.*, vol. 15, pp. 1159–1162, 2015.
[39] A. Edalati and W. McCollough, "A novel dual-band beam-switching antenna based on active frequency selective surfaces," in *Proc. IEEE Int. Symp. Antennas Propag. USNC/URSI Nat. Radio Sci. Meeting*, Jul. 2017, pp. 1985–1986.
[40] K. L. Chung, H. Tian, C. Song, and C. Zhang, "A study into the PIN diode-based active metasurface for beam steering applications," in *Proc. Int. Symp. Antennas Propag. (ISAP)*, Oct.//Nov. 2017, pp. 1–2.
[41] F. Gross, *Frontiers in Antennas: Next Generation Design & Engineering*, 1st ed. New York, NY, USA: McGraw-Hill, 2011.

SYEDA I. NAQVI (S'17) received the B.Sc. degree in computer engineering and the M.Sc. degree in telecommunication engineering from the University of Engineering and Technology, Taxila, Pakistan, in 2006 and 2011, respectively, where she is currently an Assistant Professor with the ACTSENA research group. She is involved in the design and implementation of multiple antenna array systems for current 4G and next generation millimeter-wave 5G mobile communication applications. She has authored or coauthored numerous technical articles in ISI-indexed journals and international conferences.

AQEEL H. NAQVI (S'14) received the B.S. degree in electrical (telecommunication) engineering from the COMSATS Institute of Information Technology (CIIT), Islamabad, Pakistan, in 2011, and the M.S. degree in electrical (RF and microwave) engineering from the School of Electrical Engineering and Computer Sciences (SEECS), National University of Sciences and Technology (NUST), Islamabad, Pakistan, in 2015. He is currently pursuing the Ph.D. degree with the School of Electrical and Electronics Engineering, Chung-Ang University, Seoul, South Korea. His research interests include design and analysis of microwave and millimeter-wave antennas, reconfigurable antennas, and planar and 3D printed antennas.

FARZANA ARSHAD received the B.Sc. degree in software engineering and the M.Sc. degree in telecommunication engineering from the University of Engineering and Technology, Taxila, in 2006 and 2010, respectively, where she is currently a part time Ph.D. Scholar with the ACTSENA group. Her research interests include low profile multi-band and reconfigurable antenna arrays.

MUHAMMAD A. RIAZ received the B.S. and M.S. degrees in electrical engineering from Iowa State University, USA, in 2009 and 2010, respectively, where he joined the Department of Electrical and Computer Engineering as a Research Assistant. He is currently as Assistant Professor with the ACTSENA research group, University of Engineering and Technology, Taxila. He is also the Director of Electronics and Measurements laboratory, Department of Electrical and Computer Engineering. He is involved in the design and implementation of chipless RFID tags based on electromagnetic signature and their signal processing applications. His research work has been featured in a number of ISI-indexed journals.

MUHAMMAD A. AZAM received the B.Sc. degree in computer engineering from the University of Engineering and Technology (UET) Taxila, Pakistan, in 2006, the M.Sc. degree (Hons.) in wireless networks from Queen Mary University, London, U.K., in 2008, and the Ph.D. degree in pervasive and ubiquitous computing from London, in 2012. From 2006 to 2007, he was a Lecturer with UET Taxila, Pakistan, where he has been an Assistant Professor with the Department of Computer Engineering, since August 2013. From May 2012 to July 2013, he was the Head of Academics with the Cromwell College of IT and Management, London. He leads a research team of M.S. and Ph.D. Students in the area of pervasive and ubiquitous computing. His research interest includes network architecture, communication protocols, network security, embedded systems, ambient intelligence, wireless communications, opportunistic networks, and recommender systems.

MANSOOR S. KHAN received the B.Sc. degree from PU Lahore, Pakistan, in 1994, the M.Sc. degree in statistics from the University of ARID Agriculture Rawalpindi, Pakistan, in 2000, and the Ph.D. degree from the Beijing Institute of Technology (BIT), China, in January 2016. He is currently an Assistant Professor with the Department of Mathematics, COMSATS University, Islamabad, Pakistan. He has more than ten research papers in reputed journals and proceedings of international conferences. His research interests include mathematical modeling and optimization, quality and reliability engineering, survival analysis, spatial data analysis, and data science. He received the National Research Program for Universities award from HEC, Pakistan.

YASAR AMIN received the B.Sc. degree in electrical engineering with specialization in telecommunication, the MBA degree in innovation and growth from the Turku School of Economics, University of Turku, Finland, the M.Sc. degree in electrical engineering with specialization in system on chip design, and the Ph.D. degree in electronic and computer systems from the Royal Institute of Technology (KTH), Sweden, with the research focus on printable green RFID antennas for embedded sensors. He is currently an Associate professor and the Chairman of the Telecommunication Engineering Department, University of Engineering and Technology Taxila, Pakistan. He is also the Director of the Embedded Systems Research and Development Centre. He is the Founder of Agile Creative Technologies for Smart Electromagnetic Novel Applications (ACTSENA) research group. He has authored or coauthored more than 100 international technical papers in conferences and journals. His research interests include the design and application of multiple antenna systems for next generation mobile communication systems, millimeter-wave and terahertz antenna array, implantable and wearable electronics, and inkjet printing technology in microwave applications. He is a member of more than a dozen international professional societies and a fellow of PAE.

JONATHAN LOO received the M.Sc. degree in electronics and the Ph.D. degree in electronics and communications from the University of Hertfordshire, U.K., in 1998 and 2003, respectively. He leads a research team of eight Ph.D. Students in the area of communication and networking. He is currently a Professor and the Chair of computing and communication engineering with the School of Computing and Engineering, University of West London, U.K. His research interests include network architecture, communication protocols, network security, embedded systems, video coding and transmission, wireless communications, digital signal processing, and optical networks. He has successfully graduated 13 Ph.D.'s as a Principle Supervisor and contributed over 175 publications in the aforementioned specialist areas.

HANNU TENHUNEN is currently the Chair Professor of electronic systems with the Royal Institute of Technology (KTH), Stockholm, Sweden. He has been a Full Professor, an Invited Professor or a Visiting Honorary Professor in Finland (TUT and UTU), Sweden (KTH), USA (Cornel U), France (INPG), China (Fudan and Beijing Jiaotong Universities), and Hong Kong (Chinese University of Hong Kong), and has an Honorary Doctorate from Tallinn Technical University. He has been the Director of multiple national large-scale research programs or being an Initiator and the Director of national or European graduate schools. He has actively contributed to VLSI and SoC design in Finland and Sweden via creating new educational programs and research directions, most lately at European level as being the EU-level Education Director of the new European flagship initiative European Institute of Technology and Innovations (EIT), and its Knowledge and Innovation Community EIT ICT Labs. He has been granted nine foreign patents. He has authored or coauthored more than 900 international technical papers in conferences and journals. He is a member of Academy of Engineering Science of Finland. He is the founding Editorial board member of three scientific journals and a Guest Editor for multiple special issues of scientific journals and books.